引用格式：JU Xinyan, WANG Zexu, YAN Hao, et al. Adaptive Programmable Integrated Microwave Photonic Signal Processor (Invited)[J]. Acta Photonica Sinica, 2026, 55(3):0355108
琚新琰,王泽旭,闫昊,等.自适应可编程集成微波光子信号处理器(特邀)[J].光子学报,2026,55(3):0355108

自适应可编程集成微波光子信号处理器(特邀)

琚新琰,王泽旭,闫昊,宋立甲,谢意维,戴道锌
(浙江大学 光电学院 光及电磁波研究中心,杭州 310058)

摘　要:提出了一种基于六边形网格结构的自适应可编程光子信号处理器,其单元由马赫-曾德尔干涉仪组成。该处理器凭借其灵活的拓扑重构能力,通过冠豪猪优化算法,可以实现包括非对称马赫-曾德尔干涉仪、光学环形谐振腔在内的多种滤波响应。基于此,通过配置不同自由光谱范围的鉴频单元,实现了宽带粗测与窄带精测相结合的多级协同测量方案,显著提升了测频量程与精度。此架构非常适合构建可扩展的光子系统,为实现高性能、低复杂度的光学计算与互连提供了一种切实可行的解决方案。

关键词:可编程光子处理器;马赫-曾德尔干涉仪;微波光子学;光学滤波;频率测量
中图分类号:TN252　　**文献标识码**:A　　**doi**:10.3788/gzxb20265503.0355108

0　引言

随着超高速5G/6G无线网络、超宽带雷达以及量子信息系统等前沿技术迅猛发展,对高频微波信号的产生、传输和处理能力提出了前所未有的要求。面对日益增长的带宽、速度与能效挑战,微波光子技术被认为是一种极具前景的解决方案[1-7]。该技术利用光子在集成光路中传播的超宽带特性,通过在不同光路间的干涉与复用,实现对微波信号的高精度调制、分配与处理,从而突破传统电子系统的性能瓶颈[8-13]。此外,片上可编程光子-微波信号处理器通过重构其架构,实现多功能化与灵活配置,为新一代高性能微波信号系统提供坚实的硬件支撑[14-23]。

迄今,多种基于干涉仪阵列的集成微波光子信号处理器已被实现。典型的实现方式包括采用带延迟线臂的有限冲激响应滤波器[9]、与延迟线级联的马赫-曾德尔干涉仪结构[14-17]、基于亚波长光栅波导的设计[18-19]、阵列波导光栅[19]以及级联环形谐振器等多种方案[20-23]。此外,也出现了基于一系列可调"积木式"单元构成的通用型信号处理器,能够通过软件编程灵活实现多种功能[5]。虽然通用型处理器在理论上具备强大的灵活性,但在迈向工程实用的过程中,如何平衡硬件架构的可重构性与大规模集成后的系统扩展性,依然是当前面临的核心瓶颈。目前的方案在处理复杂任务时,往往受限于固定的互连拓扑,导致在应对多功能切换或高精度信号处理时,系统架构的复杂程度与功能实现的直接性之间存在明显制约。这种架构上的局限性,限制了集成光子处理器在多变应用场景下的实际部署能力。

本文实现了一种自适应MZI的六边形网格结构可编程光子信号处理器。本研究通过实现微波光子学中的两种典型功能——拓扑结构滤波器和微波频率测量,对所提出的架构进行了实验验证。通过冠豪猪优化算法,利用其高度灵活的拓扑重构特性,能够根据任务需求快速构建出非对称马赫-曾德尔干涉仪、光学环形谐振腔等多种典型的滤波响应。在此基础上,本文验证了一套高效的微波频率测量方案,通过在网格中灵活配置不同自由光谱范围的鉴频单元,实现了宽带粗测与窄带精测相结合的多级协同测量,显著提升了测频的精度与量程。结果表明该架构为实现自适应的高性能光子集成网络提供了可行路径,为增强系统功

基金项目:国家自然科学基金(62175214),浙江省自然科学基金(LDT23F04012F05, LDT23F04015F05, LDT23F04014F01),中央高校基本科研业务费(226202400171).
第一作者:琚新琰,22330110@zju.edu.cn
通讯作者:谢意维,xieyiw@zju.edu.cn
收稿日期:2025-11-20;**录用日期**:2026-01-05

能、精度及计算可靠性奠定了坚实基础。

1 制作与表征

图1(a)是设计的自适应六边形网状结构的系统示意图。该架构具有高度灵活性,可通过控制MZI的功率分光比来动态选择不同光路,从而实现多种功能。

该器件制备在220 nm绝缘体上硅晶圆上,硅芯层厚度为220 nm,埋氧层厚度为2 μm。如图1(b)所示,

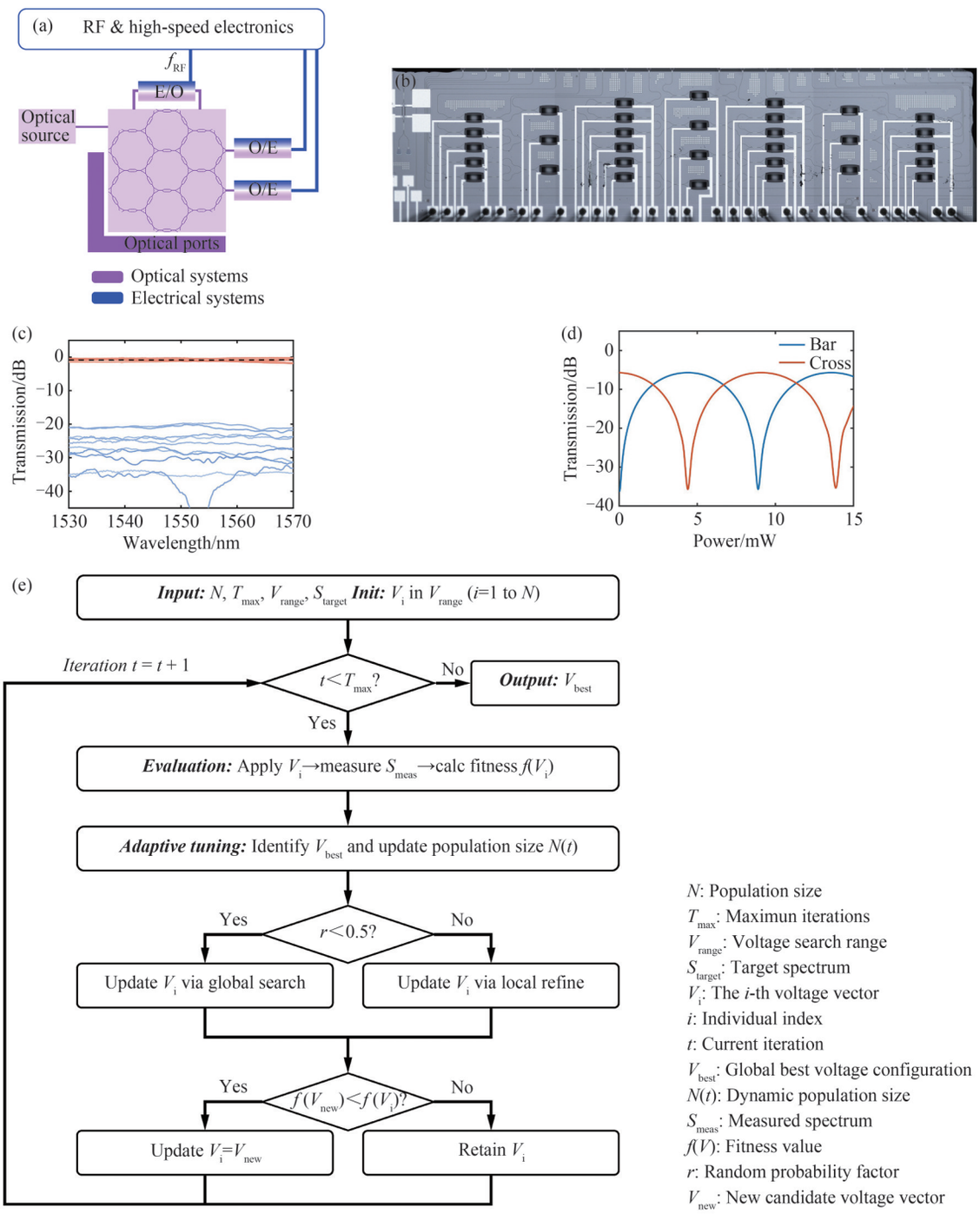


图1 系统架构图和马赫-曾德尔干涉仪标定结果。(a)处理引擎示意图;(b)制备芯片的显微照片;(c)10个MZI测试结构的消光比实测值;(d)交叉端口与直通端口透射率随加热功率的变化关系;(e)冠豪猪优化算法流程图

Fig.1 System architecture and calibration results of MZIs. (a) Schematic diagram of the processing engine; (b) Microscope image of the fabricated chip; (c) Measured extinction ratios of 10 MZI test structures; (d) Transmissions at the cross-and bar-ports as a function of the heating power; (e) Flowchart of the Crested Porcupine Optimizer algorithm

芯片面积约为3 mm×1 mm芯片包含32个MZI、32个热调谐器、46个焊盘和24个光学输入/输出端口。所有加热器的引线均被引导至芯片底部,以便与印刷电路板进行引线键合,其尺寸为30 mm×50 mm。对于芯片的多端口耦合,使用了一个36通道光纤阵列,测得的输入和输出耦合损耗约为15 dB。

为了验证MZI的性能,测量了10个MZI测试结构在1 530 nm至1 570 nm波长范围内的传输谱。如图1(c)所示,测试结果表明器件具有优异的消光比(>20 dB)。为量化每个MZI的半波功耗,我们在1 550 nm波长下通过将加热器功率从0扫描至15 mW测量了交叉端口和直通端口的响应。图1(d)展示了一个MZI的测试结果,产生π相位偏移所需的加热功率为4.41 mW。对于六边形网状结构的调控,我们采用了冠豪猪优化算法[24],其工作原理如图1(e)所示,主要分为初始化、闭环评估与策略演化三个阶段。首先在预设电压范围内生成随机种群,随后通过实测光谱反馈计算适应度值,并据此更新全局最优配置与动态种群规模。在演化过程中,系统依据随机概率在勘探与开发模式间切换,利用四种演化策略生成候选电压矢量,并通过贪婪更新机制确保收敛至最优电压配置。

2 系统性验证

2.1 拓扑结构滤波

提出的六边形微波光子信号处理通过编程即可实现不同滤波响应,其中非对称马赫-曾德尔干涉仪(Asymmetric MZI, AMZI)作为周期性陷波滤波器,构成了晶格滤波器和有限脉冲响应滤波器的基本单元。通过调控波导网格中的MZI器件,我们成功实现了不同两臂延迟量的AMZI($\Delta L=n\times$BUL,n=2或8),其消光比均超过25 dB,见图2,其中,对于每种结构,图中三条不同颜色的曲线分别对应通过调节作为耦合单元的MZI所实现的不同消光比结果。图2(a)和(b)分别展示了输出端口在2-BULs和8-BULs不同延迟量的条件下的实测光谱响应。自由光谱范围(Free Spectral Range,FSR)随路径不平衡量变化(2-BULs AMZI为0.64 nm,8-BULs AMZI为0.17 nm)。针对每种情况,本文验证了可调耦合比特性。通过调节两个分光MZI的耦合比,实现了消光比在25 dB至10 dB范围内的连续可调。将实验结果与传递函数的理论表达式进行了对比,获得了良好的一致性,这为后续微波频率测量链路奠定了良好基础。

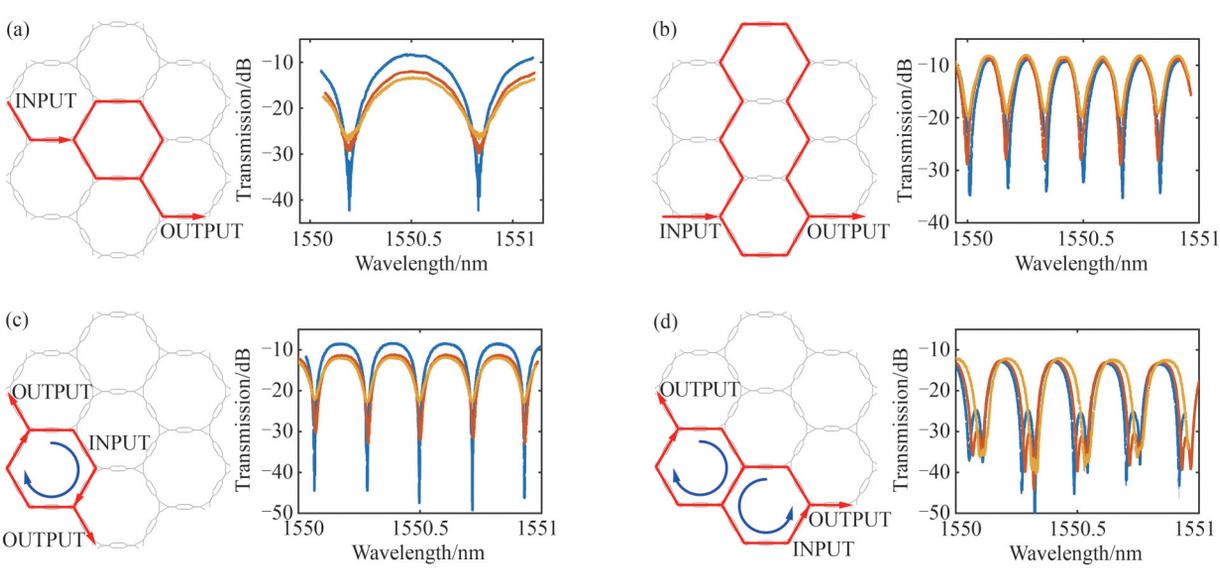


图2 拓扑结构滤波器的实验结果。(a)臂长差为2-BULs的非对称马赫-曾德尔干涉仪;(b)臂长差为8-BULs的非对称马赫-曾德尔干涉仪;(c)腔长为6-BULs的光学环形谐振腔;(d)腔长为6-BULs的二级耦合谐振光波导

Fig.2 Experimental results of the topological structure filters. (a) a 2-BULs AMZI; (b) a 8-BULs AMZI; (c) a 6-BULs ORR; (d) a 6-BULs 2-CROWs

光学环形谐振腔(Optical Ring Resonator, ORR)作为周期性陷波滤波器,构成了无限脉冲响应滤波器的基本单元。通过在波导网格中适当调控MZI器件,我们成功实现了腔长为6-BULs的单环形谐振腔响应。图2(c)展示了一个单环形谐振腔的带阻响应测试结果。测量数据对应不同的耦合比条件,其消光比可在35 dB

至10 dB范围内调节。实验结果与传递函数的理论表达式进行了对比，显示出良好的一致性。

基于腔长为6-BULs的单环形谐振腔，构建更复杂的滤波器响应，例如耦合谐振腔光波导(Coupled Resonator Optical Waveguides，CROWs)、环形辅助马赫-曾德尔干涉仪等。其中CROWs结构在光学滤波、色散补偿、光缓存及非线性光学等领域具有广泛应用[25]。该结构由一系列谐振腔构成，光波通过相邻单元间的耦合实现传输。本文验证了2级CROWs结构，并测量了其直通端口的带阻滤波响应，结果如图2(d)所示。通过与前述单环响应对比可见，在实现可调消光比的同时，随着谐振腔数量的增加，其传输谱开始呈现平坦化的特征。

2.2 频率测量

设计的可编程信号处理器可以实现不同FSR的AMZIs(如图2(a)和(b))，其响应斜率随对应响应特性变化，因而非常适用于基于幅度比较函数(Amplitude Comparison Function，ACF)的微波频率测量。我们构建了一种可动态识别宽带频率变化信号的光子频率测量系统。该系统由一个实现双边带载波抑制调制的马赫-曾德尔调制器(Mach-Zehnder Modulator，MZM)和一组具有不同FSR的AMZI频率鉴别器组成，可分别实现宽带粗略测量和窄带精确测量。

其原理如下：未知频率的射频信号通过外部MZM调制到光载波上，该MZM工作在零传输点以实现双边带载波抑制调制，如图3(a)所示。调制后的光信号通过具有正弦光谱响应的AMZIs滤波器。当光载波波长与AMZIs直通/交叉端口响应谱的中心对齐时，调制信号在直通/交叉端口将呈现相反的斜率响应。随后，AMZIs两个端口的输出光信号被送至两个光电探测器进行探测。最终通过计算两路光探测器输出的比值得到ACF曲线，如图3(b)所示。所得的ACF曲线可用于估算整个测量范围内未知输入微波频率。

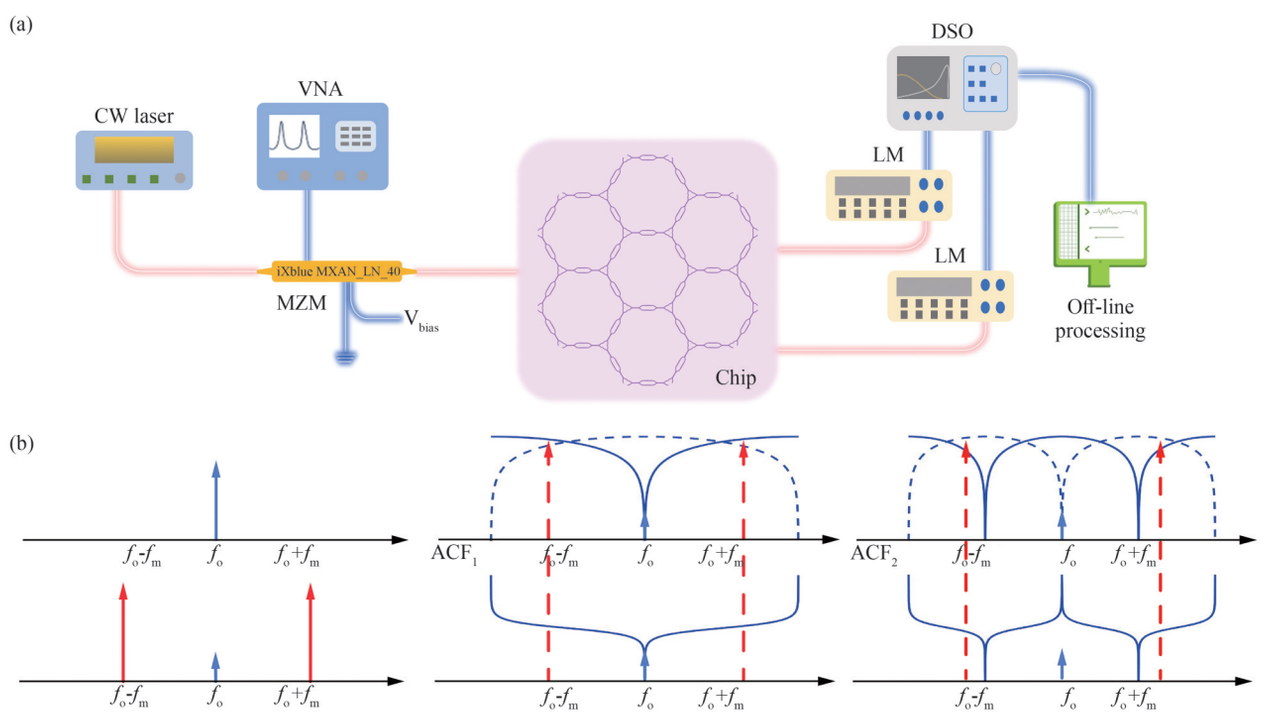


图3 频率测量系统结构图及原理。(a)微波频率识别实验装置。VNA：矢量网络分析仪；LM：光波万用表；DSO：数字存储示波器；(b)输入激光器、MZM和两个AMZIs的输出光谱，及其对应的ACF曲线

Fig.3 Schematic diagram and principle of the frequency measurement system. (a) Experimental setup to perform the microwave frequency identification. VNA: Vector Network Analyzer, LM: Lightwave Multimeter, DSO: Digital Storage Oscilloscope; (b) represents the output spectra from the input laser, MZM, two AMZIs, and their corresponding ACF curves, respectively

设AMZIs的两路输出功率分别为P_{cross}和P_{bar}，二者均与未知频率f相关。功率比P_{cross}/P_{bar}将成为输入微波频率f的函数，该函数通常称为ACF

$$\mathrm{ACF}=\frac{P_{\mathrm{cross}}}{P_{\mathrm{bar}}}\propto\frac{\sin^2(\pi f\tau)}{\cos^2(\pi f\tau)}=\tan^2(\pi f\tau) \tag{1}$$

式中,τ为AMZIs两臂间的时延差。由式(1)可知,减小FSR会增大ACF曲线的斜率绝对值,从而增强对微小频率变化的灵敏度。反之,增大FSR将扩展频率测量范围,但会降低ACF斜率绝对值,导致测量精度下降。因此,为平衡大测量范围与高精度需求,本文实现了两种不同FSR的AMZIs,其频谱图如图2(a)和2(b),其对应的FSR分别为0.64 nm和0.17 nm。具有大FSR的$\mathrm{AMZI_1}$和小FSR的$\mathrm{AMZI_2}$。这样,两种AMZI的频率测量结果可互为补充,从而实现更宽的频带覆盖和更高的测量精度。

图4(a)和(c)是两种AMZIs的测试ACF曲线。显然,$\mathrm{ACF_1}$实现约30 GHz的大带宽测量,但斜率较缓,导致测量误差较大。相比之下,$\mathrm{ACF_2}$仅能测量10 GHz频率范围,但具有较高精度。为了结合各自优势,在测量过程中,首先利用宽带$\mathrm{ACF_1}$通道对待测频率进行初步定位,通过其单调响应区间确定频率所属的子区间,从而有效消除窄带通道产生的周期模糊问题。在完成频段定位后,系统通过电压控制相位调节快速切换至窄带$\mathrm{ACF_2}$通道,在已确定的区间内完成高分辨率的精细测量。受光载波影响,$\mathrm{ACF_1}$与$\mathrm{ACF_2}$的极值比小于对应AMZI的消光比。通过抑制光载波可进一步改善该比值,从而提升测量精度。图4(b)是$\mathrm{ACF_1}$在各测试频率点估算的微波频率与实际输入频率的对比及测量误差。结果表明,该系统可测量0.01~30 GHz的宽带微波频率,均方根误差约为352 MHz。图4(d)显示了采用$\mathrm{ACF_2}$测试的微波频率,测量频率范围在$\mathrm{ACF_1}$的辅助下仍保持30 GHz。由于$\mathrm{ACF_2}$斜率更为陡峭,频率估算的均方根误差降至131 MHz。

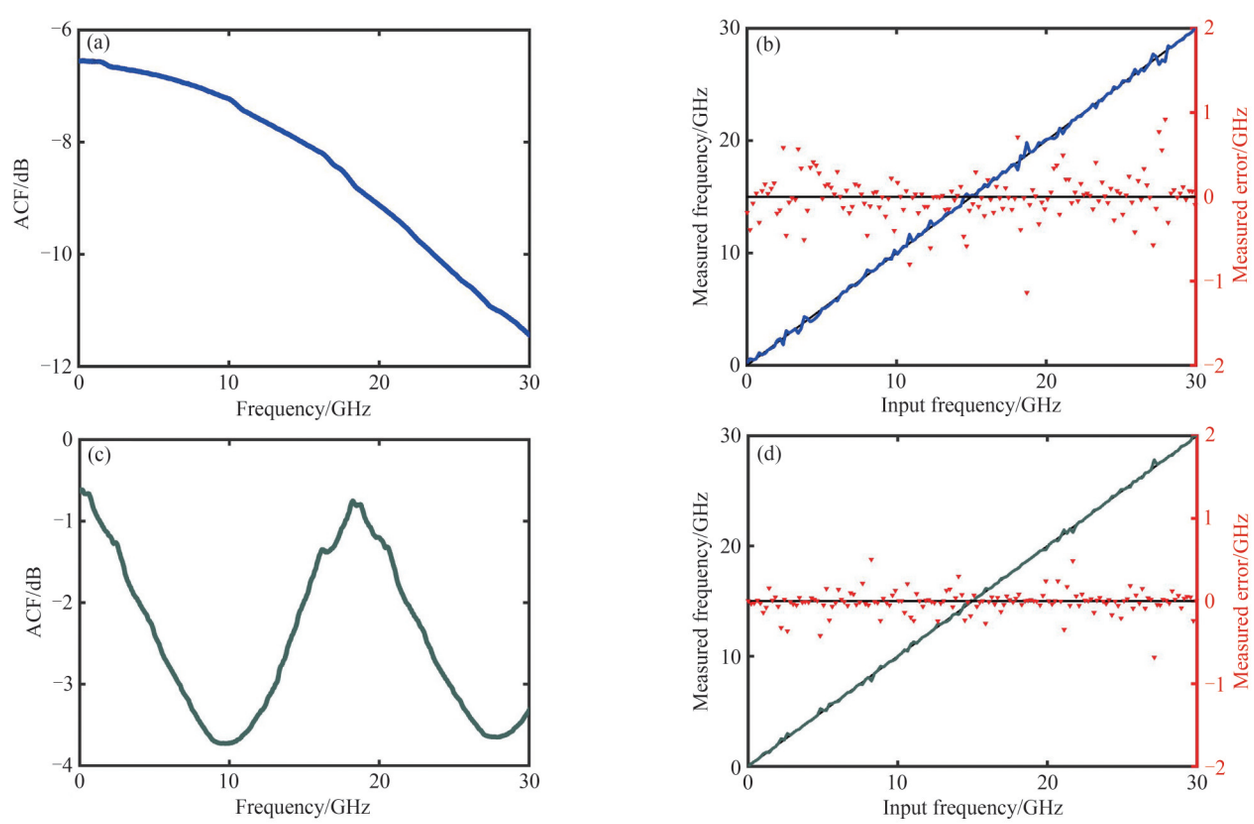


图4 频率测量结果分析。(a)$\mathrm{ACF_1}$曲线;(b)基于$\mathrm{ACF_1}$的估算频率;(c)$\mathrm{ACF_2}$曲线;(d)基于$\mathrm{ACF_2}$的估算频率

Fig.4 Frequency measurement result analysis. (a) The $\mathrm{ACF_1}$ curve; (b) Estimated frequency based on $\mathrm{ACF_1}$; (c) The $\mathrm{ACF_2}$ curve; (d) Estimated frequency based on $\mathrm{ACF_2}$

为了进一步评估所提出的可编程处理器的性能,将本方案的测量能力与当前的集成微波频率测量系统进行了基准对比。表1汇总了包括架构、测量范围和精度在内的关键指标的综合对比结果。

表1 代表性集成微波光子频率测量系统的性能对比

Table 1 Performance comparison of representative integrated microwave photonic frequency measurement systems

Ref	Platform	Dynamic measurement	Measurement range/GHz	Error/MHz	FOM	Reconfigurability
[26]	Si_3N_4	N	0.5～4	93.6	2.674	N
[27]	InP	N	5～15	＜200	＜2	N
[28]	As_2S_3	N	38	1	2.63e-3	N
[29]	SOI	N	0～40	318.9	0.797	N
[30]	SOI	N	1.6～40	＜60	0.156	N
[31]	SOI	Y	2～34	10.85	0.033	N
[32]	SOI	Y	10～20	409.4	4.094	N
[33]	TFLN	Y	2～67	123	0.189	N
[34]	SOI	N	20	-	-	Y
This work	SOI	N	30	131	0.437	Y

Y, yes; N, no; FOM, Measurement error as a percentage of the total measurement range.

3 应用扩展

为应对未来通信/雷达系统对复杂频谱场景下大带宽、高精度、实时测频的需求，基于已初步验证的小规模六边形芯片架构，可进一步展望其大规模扩展应用的巨大潜力。该架构高度模块化与可重构的核心特性，使其为构建复杂电磁环境下的多功能、自适应测量系统提供了清晰的演进路径。在实现更大带宽测量的过程中，需要结合可编程信道化阵列与可编程鉴频器网络高效协同设计技术，使系统在芯片规模持续扩展的同时，仍能保持优异的功能扩展性与参数可调性，其整体概念如图5所示。

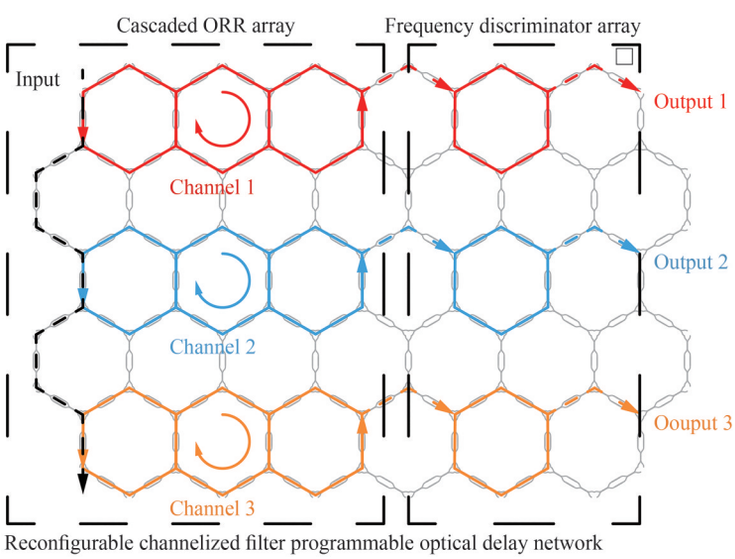


图5 大规模可重构信道化鉴频器

Fig.5 Large-scale reconfigurable channelized frequency discriminator

其中，可编程信道化阵列将基于六边形拓扑集成大规模级联微环谐振腔，通过近似方形响应的级联微环谐振腔滤波组阵列，将超宽带信号高效划分为多个频谱子带，实现对各子带的并行测量。该规整、重复的拓扑结构在芯片布局与布线层面具有显著优势，可有效支撑信道数量的进一步提升。通过对各六边形单元内微环耦合系数的统一与精细调控，可实现对超宽带频谱的灵活划分与动态管理。在此基础上，各信道不仅能够保持平顶滤波的优良频谱特性，其中心频率与带宽亦可实现独立、连续的可编程重构，从而为后级信号处理提供高度精细且可定制的频谱切片。

经信道化后的信号将进一步被路由至规模同步扩展的可编程鉴频器网络。该网络由大量可独立编程的AMZI鉴频单元构成。在大规模系统中，可针对不同信道或信道集群配置不同的干涉臂长度差，使信道化频谱并行输入鉴频器网络。通过调节AMZI两臂的相对延迟，实现不同自由光谱范围的设定，从而支持高精

度细测与宽范围粗测等多种测频模式的并行运行，显著增强系统对复杂、多变信号场景的适应能力。最终，各鉴频单元的输出由高灵敏度光电探测器阵列统一接收，并结合可编程网络的全局配置状态进行数据融合与协同处理，实现对全频域范围内复杂波形的高精度、高动态、同步测量。

尽管本文的研究重点在于频率测量功能，但选择六边形波导网格架构的核心动因是构建一个通用型可编程微波光子处理器。频率测量仅作为验证该芯片编程逻辑与硬件重构能力的典型案例。

为了直观展示该平台的应用潜力，表2总结了当前微波光子学领域中由专用光子集成电路（ASPICs，Application Specific Photonic Integrated Circuits）所覆盖的主流应用场景。虽然ASPICs在特定功能上具有优异的性能指标，但其硬件结构通常是固化的，仅能执行单一任务。相比之下，本文提出的通用架构凭借其高维度的重构能力，理论上能够在同一硬件平台上通过软件定义覆盖表1中所列的大多数ASPIC功能。

表2　微波光子系统所需的关键功能汇总

Table 2　Summary of key functionalities in microwave photonic systems

Functionality	Description	Application
Tunable RF filtering[35]	Channel selection in the RF domain & noise reduction	Mobile & satellite comms, IoT, sensing, radar, imaging
Tunable RF delay line[36]	Selective RF channel delay and time-delayed signal combination	Phased array antennas, radar, sensing, lidar
Frequency measurement[37]	Identification of the frequency of non-desired interfering signals	Radar, navigation systems, self-interference cancellation
Optoelectronic oscillator[36]	Ultrapure tunable RF tone generation	Avionics and satellite comms, navigation systems, time and frequency measurement
Arbitrary waveform generation[36]	Generation of RF wavepackets with arbitrary amplitude shapes	Radar, mobile communications, Microwave imaging, instrumentation
Optical generation of mm-wave CW signals[36]	Baseband and intermediate frequency conversion to/from the radio spectrum	Mobile, wearable & satellite comms, radar, imaging
Beamforming[35]	Broadband angular steering of a radiation pattern	Phased array antennas, 5-6G mobile & satellite comms, sensing, radar, imaging
Tunable beam splitting[38]	Signal distribution among different physical outputs	Mobile and satellite communications

值得强调的是，该特定的六边形拓扑结构在先前的研究中已被证明[34]能够支持多种复杂的微波光子信号处理任务。为了便于读者理解这种“多功能性”的实现机制，在表2之后详细补充了这些已证实功能在该架构上的基本实现原理。这种从“专用”向“通用”的范式转变，预示着未来微波光子系统将向着高度集成化、软件定义的智能化方向演进。

为了进一步揭示该通用处理器的应用潜力，结合表2所列的关键应用场景，详细阐述该六边形波导网格架构在频率测量之外实现其他微波光子功能的物理机制与硬件逻辑。这些功能均基于该架构的可编程特性，通过对芯片内部光路拓扑的实时重构，可实现从基础的信号调控到复杂的系统级信号产生。凭借可编程波导网格灵活的拓扑重构能力，该架构作为一个通用硬件平台，能够有力支持从基础信号处理到复杂系统互连的广泛微波光子学应用。在信号处理与产生方面，该芯片不仅能通过合成复杂的光学传递函数，实现中心频率与带宽动态可调的射频滤波器及全360°连续移相器，还能利用光子横向滤波原理与高阶判据滤波技术，分别实现任意射频波形产生与高性能的毫米波频率倍增。此外，将其置于反馈环路中，通过灵活切换谐振腔路径，还可构建频率可重构的光电振荡器。针对雷达与通信基础设施，该架构利用网格合成的真时延线，能够消除宽带工作的波束斜视效应，实现宽带相控阵波束成形；同时，凭借其高维空间路由特性，该芯片还可作为核心矩阵，执行5G/6G数字化信号的动态光互连、柔性功率分配以及复杂的信号交换与分插复用任务，展现了其替代多类专用集成电路的潜力。

4　结论

综上所述，我们提出了一种基于六边形架构的自适应马赫-曾德尔干涉仪方案。所提出的六边形微波光子信号处理器通过冠豪猪优化算法，实现有限冲激响应和无限冲激响应两种滤波模式，并可灵活调节

消光比与自由光谱范围。该架构同时被应用于微波频率测量,展现了宽带扫描与高精度探测相结合的综合性能。此外,通过马赫-曾德尔干涉仪单元的增量式集成,可实现网络维度的可扩展拓展,为量子信息处理和高维光信号操控等复杂应用提供支撑。可以预见此架构有望构建更大规模的自适应系统,为高性能、低复杂度的大规模微波光子信号处理系统发展提供可行路径。

参考文献

[1] XIE Y, GENG Z, ZHUANG L, et al. Programmable optical processor chips: toward photonic RF filters with DSP-level flexibility and MHz-band selectivity[J]. Nanophotonics, 2018, 7(2): 421-454.

[2] PÉREZ D, GASULLA I, CRUDGINGTON L, et al. Multipurpose silicon photonics signal processor core[J]. Nature Communications, 2017, 8(1): 636.

[3] LIU Y, CHOUDHARY A, MARPAUNG D, et al. Integrated microwave photonic filters[J]. Advances in Optics and Photonics, 2020, 12(2): 485-555.

[4] FENG H, GE T, GUO X, et al. Integrated lithium niobate microwave photonic processing engine[J]. Nature, 2024, 627(8002): 80-87.

[5] BOGAERTS W, PÉREZ D, CAPMANY J, et al. Programmable photonic circuits[J]. Nature, 2020, 586(7828): 207-216.

[6] YIN Yuexin, XU Xinru, DING Yingzhi, et al. Progress and challenge of 3D photonic integrated circuit (invited)[J]. Acta Photonica Sinica, 2022, 51(7): 0751416.
尹悦鑫, 许馨如, 丁颖智, 等.三维光子集成芯片的进展与挑战(特邀)[J].光子学报,2022, 51(7): 0751416.

[7] LIU Xiaoteng, FENG Jijun, WU Xinyao, et al. Silicon waveguide based integrated optical phased array chips (invited)[J]. Acta Photonica Sinica, 2020, 49(11): 1149012.
刘晓腾, 冯吉军, 吴昕耀, 等.基于硅基波导的集成光学相控阵芯片(特邀)[J].光子学报,2020, 49(11): 1149012.

[8] YANG L, NIE J, DUAN L. Dynamic optical sampling by cavity tuning and its application in lidar[J]. Optics Express, 2013, 21(3): 3850-3860.

[9] XIE Y, ZHUANG L, LOWERY A J. Picosecond optical pulse processing using a terahertz-bandwidth reconfigurable photonic integrated circuit[J]. Nanophotonics, 2018, 7(5): 837-852.

[10] VANDOORNE K, MECHET P, VAN VAERENBERGH T, et al. Experimental demonstration of reservoir computing on a silicon photonics chip[J]. Nature Communications, 2014, 5(1): 3541.

[11] LVOVSKY A I, SANDERS B C, TITTEL W. Optical quantum memory[J]. Nature Photonics, 2009, 3(12): 706-714.

[12] KHONINA S N, KAZANSKIY N L, BUTT M A, et al. Optical multiplexing techniques and their marriage for on-chip and optical fiber communication: a review[J]. Opto-Electronic Advances, 2022, 5(8): 210127.

[13] GAUTHIER D. Slow light brings faster communications[J]. Physics World, 2005, 18(12): 30.

[14] XIE J, ZHOU L, LI Z, et al. Seven-bit reconfigurable optical true time delay line based on silicon integration[J]. Optics Express, 2014, 22(19): 22707-22715.

[15] WANG X, ZHOU L, LI R, et al. Continuously tunable ultra-thin silicon waveguide optical delay line[J]. Optica, 2017, 4(5): 507.

[16] MOREIRA R L, GARCIA J, LI W, et al. Integrated ultra-low-loss 4-bit tunable delay for broadband phased array antenna applications[J]. IEEE Photonics Technology Letters, 2013, 25(12): 1165-1168.

[17] CHENG S, XIA T, LIU M, et al. Composite spiral zone plate[J]. Ieee Photonics Journal, 2019, 11(1): 4500111.

[18] WANG Y, SUN H, KHALIL M, et al. On-chip optical true time delay lines based on subwavelength grating waveguides[J]. Optics Letters, 2021, 46(6): 1405-1408.

[19] SUN H, WANG Y, CHEN L R. Integrated discretely tunable optical delay line based on step-chirped subwavelength grating waveguide Bragg gratings[J]. Journal of Lightwave Technology, 2020, 38(19): 5551-5560.

[20] YARIV A, XU Y, LEE R K, et al. Coupled-resonator optical waveguide:? a proposal and analysis[J]. Optics Letters, 1999, 24(11): 711-713.

[21] XIE J, ZHOU L, ZOU Z, et al. Continuously tunable reflective-type optical delay lines using microring resonators[J]. Optics Express, 2014, 22(1): 817-823.

[22] SHAN W, LU L, WANG X, et al. Broadband continuously tunable microwave photonic delay line based on cascaded silicon microrings[J]. Optics Express, 2021, 29(3): 3375.

[23] CARDENAS J, FOSTER M A, SHERWOOD-DROZ N, et al. Wide-bandwidth continuously tunable optical delay line using silicon microring resonators[J]. Optics Express, 2010, 18(25): 26525-26534.

[24] ABDEL-BASSET M, MOHAMED R, ABOUHAWWASH M. Crested porcupine optimizer: a new nature-inspired metaheuristic[J]. Knowledge-Based Systems, 2024, 284: 111257.

[25] XIA F, SEKARIC L, O'BOYLE M, et al. Coupled resonator optical waveguides based on silicon-on-insulator photonic wires[J]. Applied Physics Letters, 2006, 89(4): 041122.

[26] MARPAUNG D. On-chip photonic-assisted instantaneous microwave frequency measurement system [J]. IEEE Photonics Technology Letters, 2013, 25(9): 837-840.
[27] FANDINO J S, MUNOZ P. Photonics-based microwave frequency measurement using a double-sideband suppressed-carrier modulation and an InP integrated ring-assisted mach-zehnder interferometer filter [J]. Optics Letters, 2013, 38(21): 4316-4319.
[28] JIANG H, MARPAUNG D, PAGANI M, et al. Wide-range, high-precision multiple microwave frequency measurement using a chip-based photonic brillouin filter[J]. Optica, 2016, 3(1): 30-34.
[29] PAGANI M, MORRISON B, ZHANG Y, et al. Low-error and broadband microwave frequency measurement in a silicon chip[J]. Optica, 2015, 2: 751-756.
[30] CHEN Y, ZHANG W, LIU J, et al. On-chip two-step microwave frequency measurement with high accuracy and ultra-wide bandwidth using add-drop micro-disk resonators[J]. Optics Letters, 2019, 44(10): 2402.
[31] TAO Y, YANG F, TAO Z, et al. Fully on-chip microwave photonic instantaneous frequency measurement system[J]. Laser & Photonics Reviews, 2022, 16(11): 2200158.
[32] YAO Y, ZHAO Y, WEI Y, et al. Highly integrated dual-modality microwave frequency identification system[J]. Laser & Photonics Reviews, 2022, 16(10): 2200006.
[33] YAN H, WANG Z, WANG S, et al. Thin-film-lithium-niobate photonic chip for ultra-wideband and high-precision microwave frequency measurement[J]. Laser & Photonics Reviews, 2025, 19(5): 2401273.
[34] PÉREZ-LÓPEZ D, GUTIERREZ A, SÁNCHEZ D, et al. General-purpose programmable photonic processor for advanced radiofrequency applications[J]. Nature Communications, 2024, 15(1): 1563.
[35] MARPAUNG D, YAO J, CAPMANY J. Integrated microwave photonics[J]. Nature Photonics, 2019, 13(2): 80-90.
[36] ZOU X, LU B, PAN W, et al. Photonics for microwave measurements[J]. Laser & Photonics Reviews, 2016, 10(5): 711-734.
[37] CHANG M P, BLOW E C, SUN J J, et al. Integrated microwave photonic circuit for self-interference cancellation[J]. IEEE Transactions on Microwave Theory and Techniques, 2017, 65(11): 4493-4501.
[38] BOGAERTS W, PÉREZ D, CAPMANY J, et al. Programmable photonic circuits[J]. Nature, 2020, 586(7828): 207-216.

Adaptive Programmable Integrated Microwave Photonic Signal Processor (Invited)

JU Xinyan, WANG Zexu, YAN Hao, SONG Lijia, XIE Yiwei, DAI Daoxin
(*State Key Laboratory of Extreme Photonics and Instrumentation, Zhejiang Key Laboratory of Optoelectronic Information Technology, College of Optical Science and Engineering, Zhejiang University, Hangzhou* 310058, *China*)

Abstract: With the explosive growth of next-generation information technologies, such as ultra-high-speed 5G/6G wireless communication networks, ultra-wideband radar systems, and quantum information processing, the requirements for the generation, transmission, and manipulation of high-frequency microwave signals have reached unprecedented levels. Facing the escalating challenges of bandwidth, speed, and energy efficiency, Integrated Microwave Photonics (IMWP) has emerged as a transformative solution. By leveraging the ultrawideband characteristics of photons propagating within integrated circuits, IMWP achieves high-precision modulation, distribution, and processing of microwave signals through interference and multiplexing across diverse optical paths, thereby surmounting the performance bottlenecks inherent in traditional electronic systems. Furthermore, on-chip programmable photonic-microwave signal processors provide a robust hardware foundation for next-generation high-performance microwave systems by reconfiguring their internal architectures to achieve multi-functionality and flexible configuration. Although various architectures based on interferometer arrays, such as finite impulse response filters with delay-line arms and cascaded ring resonators, have been demonstrated, a critical bottleneck hindering their engineering transition is the difficulty in balancing architectural reconfigurability with system scalability in complex application scenarios. Conventional designs often suffer from fixed interconnection topologies and a lack of directness in functional implementation, which constrains their practical deployment in diverse and dynamic environments.

Addressing these limitations, this work proposes and experimentally demonstrates an adaptive programmable integrated photonic signal processor based on a hexagonal waveguide mesh topology. The processor utilizes Mach-Zehnder Interferometers (MZIs) as fundamental tuning units, featuring an optimized physical-layer design to ensure high-fidelity functional mapping across the network. The device was fabricated on a 220 nm Silicon-on-Insulator (SOI) platform, with a compact footprint of approximately 3 mm×1 mm, integrating 32 tunable MZIs, 32 thermo-optic phase shifters, and 24 optical I/O ports. Comprehensive characterization of the MZI test structures reveals excellent performance, including extinction ratios exceeding 20 dB and a half-wave heating power of 4.41 mW. A central innovation of this study is the implementation of a self-adaptive control framework driven by the Crested Porcupine Optimizer (CPO) algorithm. The operational logic of the CPO-based configuration is divided into three distinct phases: initialization, closed-loop evaluation, and strategy evolution. By generating a random population within the predefined voltage range and iteratively calculating fitness values based on real-time experimental spectral feedback, the system autonomously converges to the optimal voltage configuration. During the evolution process, the algorithm dynamically toggles between exploration and exploitation modes using four distinct evolutionary strategies, ensuring both global search coverage and local refinement precision. This self-adaptive framework enables the processor to achieve immediate operational readiness with minimal control complexity, establishing a highly stable hardware-software co-design for universal signal processing.

Experimentally, the fabricated processor was configured to demonstrate two representative microwave photonic functionalities: topological filtering and frequency measurement. In the topological filtering experiments, the mesh's high degree of reconfigurability was leveraged to synthesize diverse spectral responses, including both Finite Impulse Response (FIR) and Infinite Impulse Response (IIR) filters. By precisely controlling the power splitting ratios and phase shifts within the hexagonal units, we successfully realized Asymmetric MZIs (AMZIs) with tunable extinction ratios exceeding 25 dB and Free Spectral Ranges (FSR) ranging from 0.17 nm to 0.64 nm. Furthermore, Optical Ring Resonators (ORRs) with a 6-BUL (Basic Unit Length) cavity and two-stage Coupled Resonator Optical Waveguides (CROWs) were implemented, demonstrating the mesh′s capability to synthesize complex recursive structures with flattened transmission spectra. For frequency measurement, a broadband frequency identification system was constructed using an Amplitude Comparison Function (ACF) based on a Carrier-Suppressed Single-Sideband (CS-SSB) modulation scheme. The system utilized the mesh′s ability to switch between multi-stage frequency discrimination channels with different FSRs. By synergistically combining the results from a wideband coarse-measurement channel and a narrowband high-precision channel, the system achieved a broad frequency identification range from 0.01 GHz to 30 GHz with a significantly improved Root Mean Square Error (RMSE) of 131 MHz. This collaborative measurement scheme effectively eliminates the periodic ambiguity typical of narrowband discriminators while maintaining high resolution across the entire spectrum.

In summary, this work provides a viable and scalable pathway for realizing high-performance, low-complexity integrated microwave photonic systems. The hexagonal mesh architecture demonstrates exceptional functional adaptability and structural scalability, marking a paradigm shift from Application-specific Integrated Circuits (ASPICs) to software-defined universal photonic processors. Beyond the filtering and frequency measurement demonstrations, the architecture serves as a general-purpose hardware platform capable of supporting diverse tasks, including tunable delay lines for wideband beamforming, arbitrary waveform generation, and reconfigurable optoelectronic oscillators. Theoretical analysis and experimental validation suggest that this self-adaptive framework can be extended to larger-scale networks, providing a clear evolutionary path for multi-functional, adaptive measurement systems in complex electromagnetic environments. The successful implementation of these functionalities on a single programmable chip paves the way for the future deployment of integrated photonics in advanced radar systems, 5G/6G communication infrastructures, and high-dimensional optical signal manipulation.

Key words: Programmable photonic processor; Mach-Zehnder interferometer; Microwave photonics; Optical filter; Frequency measurement

OCIS Codes: 230.3120; 220.4000; 060.2390; 230.7380

CSTR: 32255.14.gzxb20265503.0355108

Foundation item: National Natural Science Foundation of China (62175214), Zhejiang Provincial Natural Science Foundation (LDT23F04012F05, LDT23F04015F05, LDT23F04014F01), Fundamental Research Funds for the Central Universities (226202400171)